Impact of Plane Waves on Lining in Elastic Medium With Transparent Artificial Boundary

IBRAKHIM MIRZAEV[1,*], SULTAN GAYNAZAROV[2]
[1]Department of Applied Mechanics,
Tashkent State Transport University,
100167, Temiryolchilar str. 1, Tashkent,
UZBEKISTAN

[2]Faculty of Applied Mathematics and Intelligent Technologies,
National University of Uzbekistan named after Mirzo Ulugbek,
100174, University str. 4, Tashkent,
UZBEKISTAN

**Corresponding Author*

Abstract: - To effectively address dynamic problems related to underground structures subjected to wave actions, it is necessary to introduce artificial boundary conditions. Establishing conditions at these boundaries is crucial to ensure transparency of internal and external waves as they reflect off these structures. This paper proposes the use of exact non-reflective wave conditions at these boundaries. The authors explore the behavior of linings under longitudinal and shear waves using a mathematical model. The numerical implementation employs the finite element and Bathe time integration methods. Examples of circular concrete linings subjected to longitudinal and shear waves are provided. The article considers the spacing between the linings and the dimensions of the artificially defined region. The numerical results demonstrate the effectiveness and reliability of the transparency conditions at the artificial boundaries, allowing for a thorough investigation of wave impacts on underground structures under plane strain conditions.

Key-Words: - Elastic medium, Circular lining, Plane strain, Transparent boundaries, Finite element method, Bathe method.

Received: May 11, 2024. Revised: November 16, 2024. Accepted: March 9, 2025. Published: April 15, 2025.

1 Introduction

When calculating circular linings in a soil medium subjected to dynamic impacts, one crucial condition is ensuring wave non-reflection at the boundaries of the computational domain. This allows the calculation domain to be optimally limited, thus efficiently facilitating result analysis during numerical simulations.

The issue was first addressed in the article [1], which proposed formulas relating stresses to particle velocities of plane waves at artificial boundaries. It is noteworthy that Lysmer's condition and its modifications provide approximate boundary conditions. These conditions yield good results when the wavefront normal forms a right angle with the artificial boundary. In reference [2], wave energy dissipation through a non-reflective boundary was accounted for in a structure-foundation system using Lysmer's conditions and finite element methods. Similarly, the article conducted in [3] applied this method to energy dissipation during railway vehicle movement. Article [4] examined a non-uniform plane elasticity problem using finite element methods to calculate vibrations from metro trains in parallel tunnels.

Reference [5] proposed using a fictitious region with specialized wave-absorbing properties as a solution for boundary non-reflection problems. This interconnected problem, involving internal subdomains and absorbing layers, utilized heterogeneous asynchronous time integrators, facilitating the processing of absorbing layers via an explicit central difference scheme. A benchmark for three-dimensional explicit asynchronous absorbing layers modeling unbounded domains through standard displacement-based finite element methods was presented.

Paper [6] introduced a novel inversion method for reconstructing complex, incoherent SH incident

wavefields in truncated domains using wave-absorbing boundary conditions through partial differential equations constrained by optimization methods.

The review article [7] presented various models implementing non-reflective boundary conditions in bounded domains. Article [8] introduced a new approach for incorporating free-field effects into soil-structure seismic interaction (SSSI) models using 8-node finite elements bounded by compatible infinite absorbing elements.

In reference [9], transparent boundary conditions for a one-dimensional wave equation were proposed, with numerical implementation using finite difference methods. This approach was extended to three-dimensional wave equations with radial symmetry.

Studies conducted in [10], [11] and [12] give static stress analyses of various metro tunnel linings and numerical results based on tunnel embedment depth. Article [13] investigated culvert tunnels reinforced with concrete on three sides, performing frequency analyses using finite element methods. Reference [14] reviewed dynamic soil-structure interaction (SSI) methods for buildings, highlighting prevalent modeling and computational approaches and comparing their strengths, limitations, and applications.

Exact non-reflecting boundary conditions for external wave equations using boundary integral equations were proposed in [15].

Article [16] explored longitudinal wave propagation in a soil medium with surface embankments, accounting for artificial boundary transparency. The authors applied transparency conditions enhanced by additional terms associated with shear stresses.

Incorrect modeling of internal wave non-reflective conditions on artificial boundaries can lead to wave diffraction, generating parasitic waves that disrupt wave propagation within bounded regions. According to the article [17], undesirable diffraction processes occur at boundaries when the wave normal vector, defining wave propagation direction, makes an angle of less than 15 degrees with the artificial boundary.

Reference [18] analyzed the behavior of buildings under seismic excitation using modal superposition and direct integration methods, comparing responses via reaction spectra. The authors proposed the least conservative method for calculating Rayleigh damping coefficients for time-domain analyses.

The seismic impact on the floor response spectra of two adjacent reinforced concrete structures exhibiting inelastic behavior was evaluated in [19]. It demonstrated significant effects on floor acceleration spectra, enhancing acceleration propagation across a broader range of periods, particularly exciting low and moderate vibration periods.

In the article [20], they propose an accurate and robust formulation for modeling the interaction of train/bridge subsystems. Using a one-dimensional finite element formulation, a series of equations is constructed by modeling the girder structure. In addition, the equations for the suspended mass are first discretized using Newmark finite-difference formulas.

A review of the literature sources reveals no studies that precisely address non-reflective wave conditions at boundaries. This current research establishes exact transparency conditions at boundaries, ensuring unhindered wave transmission and facilitating precise modeling within bounded domains.

2 Problem Formulation

We consider a two-dimensional isotropic, linearly elastic half-plane body limited by the domain Ω, containing one or two circular linings (Figure 1).

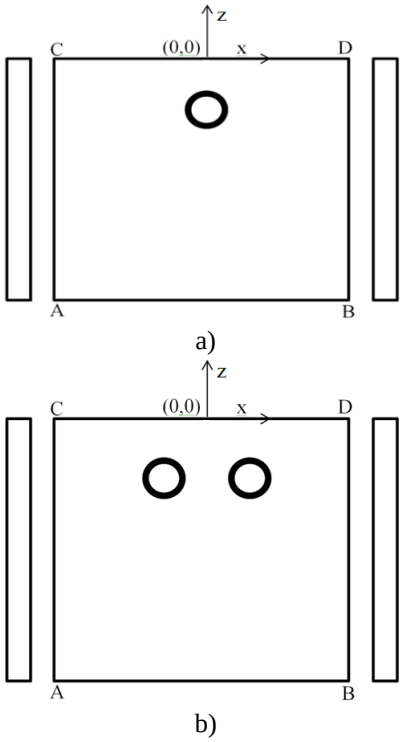

Fig. 1: Representation of main and auxiliary domains, a) medium with one lining, b) medium with two linings

Plane longitudinal or transverse waves enter the domain Ω through boundary AB, while boundaries AC and BD compensate for the truncated part of the

half-plane. The boundary CD of domain **Ω** is stress-free, implying a free surface condition at this boundary. Circular linings might be positioned at varying depths within the rectangular domain relative to the free surface.

To address the problem, we use the weak (variational) form of the equilibrium equations, [21]:

$$\int_{\Omega} [\lambda div(u) div(\delta u) + 2\mu\varepsilon^T \delta\varepsilon - (r - \rho\ddot{u} - c\dot{u})\delta u] d\Omega - \int_{\Gamma} P\delta u d\Gamma = 0, \quad (1)$$

where P is the surface force vector per unit area at the domain boundary, ρ is the material density, c is the viscosity parameter of the medium, r is the body force vector, $u^T = \{u_x, u_z\}$ is the displacement vector, ε is the strain tensor, and λ and μ are Lamé coefficients. Cartesian coordinate axes are Ox-oriented from left to right and Oz-oriented from bottom to top, with the origin at the center of the free surface.

Transparent boundary conditions are derived by applying exact solutions for plane waves relating strain and particle velocities and substituting these into the generalized Hooke's law. Additionally, solutions from corresponding one-dimensional dynamic problems for domains without linings are utilized.

Boundary conditions, when longitudinal and transverse waves enter the domain **Ω** through the boundary AB with particle velocities $f_p(t)$ and $f_s(t)$, are given by:

transparent conditions on AB:

$$P_z = -\sigma_{zz} = -c_p\rho\dot{u}_z - \lambda\frac{\partial u_x}{\partial x} + 2c_p\rho f_p(t);$$
$$P_x = -\sigma_{xz} = -c_s\rho\dot{u}_x + 2c_s\rho f_s(t); \quad (2)$$

non-reflective conditions on CD:

$$P_z = \sigma_{zz} = -c_p\rho\dot{u}_z + \lambda\frac{\partial u_x}{\partial x};$$
$$P_x = \sigma_{xz} = -c_s\rho\dot{u}_x; \quad (3)$$

or in the case of a free surface on CD:

$$P_z = \sigma_{zz} = 0; \; P_x = \sigma_{xz} = 0; \quad (4)$$

transparent conditions on AC:

$$P_x = -\sigma_{xx} = -c_p\rho\dot{u}_x - \lambda\frac{\partial u_z}{\partial z} + c_p\rho\dot{u}_x^1;$$
$$P_z = -\sigma_{xz} = -c_s\rho\dot{u}_z + c_s\rho\dot{u}_z^1; \quad (5)$$

transparent conditions on BD:

$$P_x = \sigma_{xx} = -c_p\rho\dot{u}_x + \lambda\frac{\partial u_z}{\partial z} + c_p\rho\dot{u}_x^1;$$
$$P_z = \sigma_{xz} = -c_s\rho\dot{u}_z + c_s\rho\dot{u}_z^1. \quad (6)$$

Here, c_p, c_s are propagation velocities of longitudinal and transverse waves, respectively, and $\dot{u}_z^1$ are velocity solutions are from corresponding one-dimensional plane wave problems within the auxiliary rectangular domain, defined below.

Initial conditions at t=0 set zero particle displacements and velocities in the domain:

$$u_x = 0; \; \dot{u}_x = 0; \; u_z = 0; \; \dot{u}_z = 0. \quad (7)$$

To find $\dot{u}_x^1, \dot{u}_z^1$, auxiliary domains (Figure 1) are introduced to calculate wave propagation with physical characteristics identical to **Ω**, defined by:

$$\Omega_1 = \{(x,z): x \in [0, \Delta L], \; z \in [0, -H]\},$$
$$\Gamma_{l1} = \{(x,z): x = 0, \; z \in [0, -H]\},$$
$$\Gamma_{r1} = \{(x,z): x = \Delta L, \; z \in [0, -H]\},$$
$$\Gamma_{b1} = \{(x,z): x \in [0, \Delta H], \; z = -H\},$$
$$\Gamma_{t1} = \{(x,z): x \in [0, \Delta H], \; z = 0\}.$$

For the auxiliary task, the calculation domain width L can be limited to the size of one finite element matching the boundary element size in the main domain, while the domain height H equals that of the main domain. The finite element discretization should align with the discretization at the corresponding boundary in the main domain.

Boundary conditions for a longitudinal wave at boundary Γ_{b1} are:

$$P_z = -\sigma_{zz} = -c_p\rho\dot{u}_z - \lambda\frac{\partial u_x}{\partial x} + 2c_p\rho f_p(t);$$
$$P_x = -\sigma_{xz} = -c_s\rho\dot{u}_x; \quad (8)$$

non-reflective conditions on Γ_{t1}:

$$P_z = \sigma_{zz} = -c_p\rho\dot{u}_z + \lambda\frac{\partial u_x}{\partial x};$$
$$P_x = \sigma_{xz} = -c_s\rho\dot{u}_x; \quad (9)$$

or free surface conditions:

$$P_z = \sigma_{zz} = 0;\ P_x = \sigma_{xx} = 0; \tag{10}$$

perfect sliding conditions at boundaries Γ_{l1} and Γ_{r1}:

$$u_x = 0;\ P_x = \sigma_{xz} = 0. \tag{11}$$

For a shear wave entering through the lower boundary, boundary conditions at Γ_{b1} are:

$$P_x = -\sigma_{xz} = -c_s \rho \dot{u}_x + 2c_s \rho f_s(t);$$
$$P_x = -\sigma_{zz} = -c_p \rho \dot{u}_z - \lambda \frac{\partial u_x}{\partial x}; \tag{12}$$

non-reflective conditions on Γt1:

$$P_z = \sigma_{zz} = -c_p \rho \dot{u}_z + \lambda \frac{\partial u_x}{\partial x};$$
$$P_x = \sigma_{xz} = -c_s \rho \dot{u}_x; \tag{13}$$

or free surface conditions:

$$P_z = \sigma_{zz} = 0;\ P_x = \sigma_{xz} = 0; \tag{14}$$

conditions at boundaries Γl1 and Γr1:

$$u_z = 0;\ P_x = \sigma_{xx} = 0. \tag{15}$$

Initial conditions for one-dimensional auxiliary problems match those of the main problem.

The problem formulation and boundary conditions described can be applied when medium properties vary only along the Oz axis; for instance, the medium could be layered, with each layer surface parallel to the free surface.

3 Problem Solution

Applying partial discretization with finite elements [21] to equation (1) and considering equations (1)-(7), yields a system of linear ordinary differential equations:

$$M\ddot{U} + C\dot{U} + KU = R. \tag{16}$$

With initial conditions:

$$U = 0,\ \dot{U} = 0 \text{ at t=0.} \tag{17}$$

Here, M, C, K represent the mass, damping, and stiffness matrices, respectively; U is the vector of nodal displacements; and R is the load vector.

Similarly, a system of ordinary differential equations is constructed for equations (8)-(15) in the auxiliary domain.

To solve the system of equations (16) with initial conditions (17), we use the implicit finite difference method, [22].

The solution algorithm proceeds as follows: at each time step, particle velocities for the one-dimensional domain are determined using the described methods and respective boundary conditions. These calculated particle velocities are then substituted into the corresponding boundary conditions of the main medium. Subsequently, the required values in the main domain are calculated with the same time step.

3.1 Numerical Results and Interpretations

To substantiate the proposed mathematical model, calculations of displacements, velocities, and stresses were performed in a rectangular domain measuring 100 m x 50 m and a corresponding one-dimensional domain with a height of 50 m. The domain represents homogeneous soil characterized by Young's modulus of E=1500 MPa, Poisson's ratio ν=0.3, and density ρ=2000 kg/m³. The lining is modeled as a reinforced concrete ring with an external diameter of 6 m, thickness of 0.3 m, Young's modulus E=2000 MPa, Poisson's ratio ν=0.3, and density ρ=2500 kg/m³. In simulations, the ring center is located at a depth of z=-10 m and x=0. For cases with two linings symmetrically positioned about the Oz axis at the same depth, the centers are separated by a distance L_{int}. The considered values are L_{int}=8 m, L_{int}=10 m, L_{int}=12 m, L_{int}=16 m, and L_{int}=24 m. The time step used is Δt=0.001 s, and the total simulation time is T=2 s.

As an example, the incident longitudinal wave is defined as $f_p = A(t)\cos(2\pi\omega t)$, where $A(t) = A_0 t/t_0$ for $t < t_0$, and $A(t) = A_0$ otherwise, with t_0 representing the specified wave buildup interval, A_0 the amplitude, and ω the frequency of the harmonic wave. The parameters chosen for the simulations are A_0=1 m/s, t_0=0.5 s, and ω=2 Hz. The transverse wave is similarly defined as f_s=0.

The simulations were implemented using the freely distributed finite element software system FreeFem++ [23], employing triangular six-node finite elements with second-order accuracy.

The finite-element mesh structure is illustrated in Figure 2.

Figure 3 depicts particle velocity variations within the lining and surrounding soil when subjected to a longitudinal wave at the lower boundary and the stress-free upper boundary. It can be observed from this figure that the maximum velocity reaches

2 m/s. This outcome occurs because the free surface is 10 m from the center of the lining, and the wavelength is 502.4 m. Consequently, the incident and reflected waves overlap, effectively doubling the particle velocity amplitude within the wave.

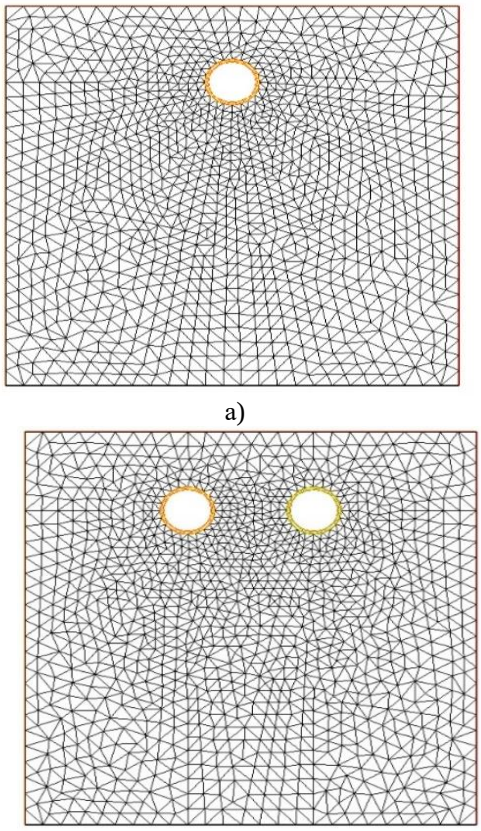

a)

b)

Fig. 2: Finite-element mesh structure of the domain: a) single lining; b) two linings

The mass of the lining is relatively small compared to the corresponding soil volume occupied by the tunnel, allowing the long wave to easily carry the lining with minimal wave diffraction.

To investigate the influence of the calculation domain width on the quality of numerical results, half-width values of the computational domain L were chosen as follows: L=7 m, L=10 m, L=20 m, L=30 m, L=40 m, L=50 m.

As seen from the plots, the velocity values are consistent across different domain widths, both in the lining and the surrounding soil, confirming the correctness of boundary transparency conditions. Additionally, the velocity amplitude is approximately twice the initial amplitude, a consequence of wave reflection from the free surface.

Figure 4 shows plots illustrating the stress intensity propagation depending on the computational domain width at two points.

The graphs demonstrate that stress intensity at the point (x=5 m, z=−10 m) remains nearly unchanged irrespective of domain width, validating the correct and precise modeling of transparent boundary conditions.

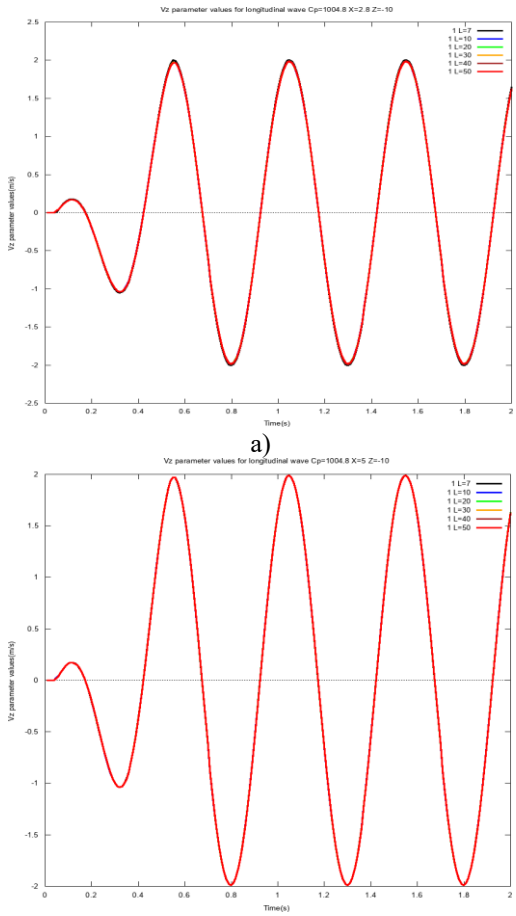

Fig. 3: Variation of the velocity component vzv_zvz for different widths of the computational domain: a) at point z=−10 m, x=2.8 m; b) at point z=−10 m, x=5 m

The stress intensity within the lining indicates minor differences for domains of smaller width compared to those with larger computational domains. This phenomenon arises from the size of finite elements at artificial boundaries, which were consistently set to 2 meters, independent of the overall domain width. However, for larger computational domains, finite elements near the lining become smaller due to an increased density of finite elements around the lining area.

Figure 5 illustrates variations in stress intensity depending on the distance between two linings, considering cases of longitudinal and shear waves. The observation point is located on the left side of the right lining, within the lining itself at

coordinates z=−-10 m and at a distance of 0.2 m from its external radius.

From the graphs, it can be observed that for longitudinal waves, the maximum stress intensity occurs at L_{int}=8 m, an intermediate intensity at L_{int}=16 m, and a significantly decreased intensity (approximately 0.02 Pa) at L_{int}=24 m. Interestingly, the maximum intensity at L_{int}=12 m exceeds the maximum at L_{int}=10 m. This behavior is explained by complex diffraction phenomena occurring near the linings, influenced by wavelength and proximity to the free surface.

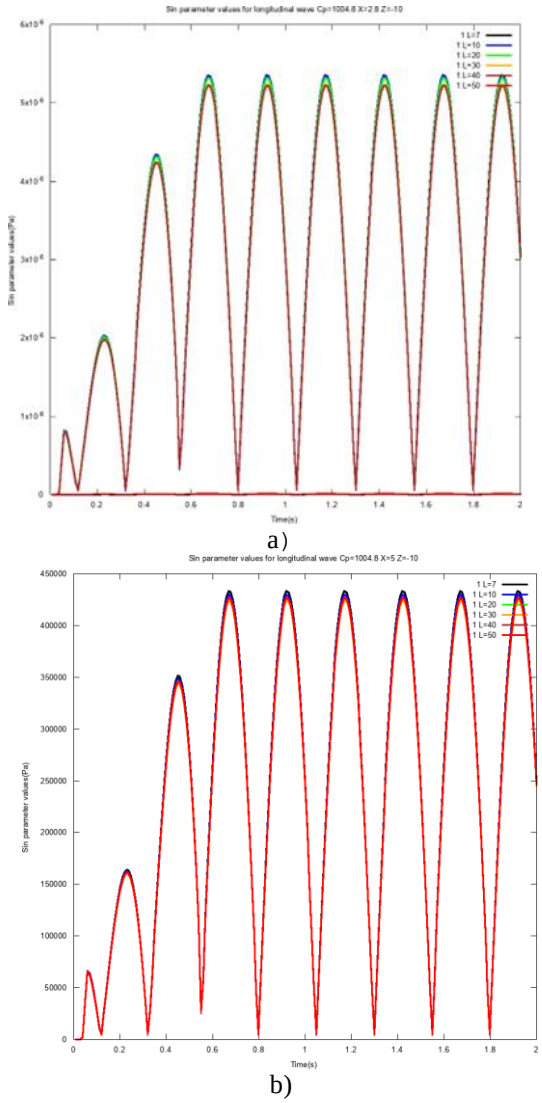

a)

b)

Fig. 4 shows plots illustrating the propagation of stress intensity depending on the computational domain width at two points: a) in the lining at point z=−10 m, x=2.8 m; b) in the soil at point z=−10 m, x=5 m

For shear waves, the highest maximum stress intensities occur at L_{int}=16 m, the lowest at: L_{int}=10 m, and intermediate maximum values at L_{int}=12 m. These results indicate that reducing the distance between linings for shear waves leads to a decrease in stress intensity.

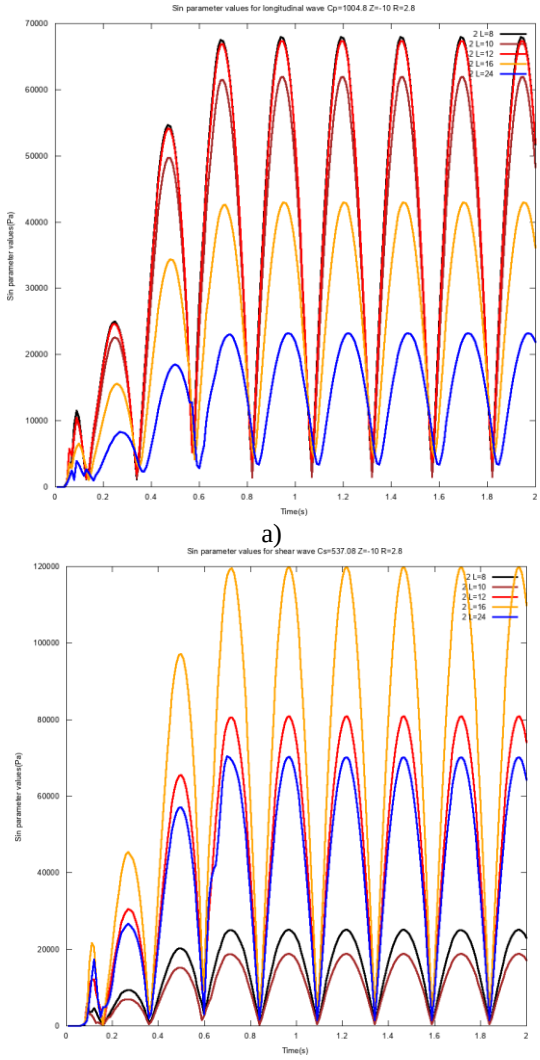

a)

b)

Fig. 5: Graphs illustrating stress intensity within the lining as a function of the distance between linings: a) for longitudinal waves; b) for shear waves

To demonstrate wave propagation in an artificially bounded domain containing one or two linings embedded in an unbounded medium, the dynamics of shear wave propagation at various moments in time are presented in the Appendix (Figure 6, Appendix).

4 Conclusion

Accurate conditions for transparent boundaries have been derived when specified longitudinal and transverse waves propagate into an artificially bounded rectangular domain parallel to its free surface. Using the open-source finite element software FreeFem++ and Bathe's method, we solved

the problem of elastic wave interaction with circular linings embedded in a homogeneous soil medium. As an illustrative example, we examined the interaction of longitudinal and transverse harmonic waves imposed at the lower transparent artificial boundary of the domain. The numerical results demonstrate the high quality of transparency conditions applied at artificial boundaries. We analyzed the dynamic response of linings at various distances between them. Under longitudinal wave excitation, increasing the distance between the linings reduces the intensity of dynamic stresses within the linings to a specific limiting value, approaching the stress intensity observed in the single-lining scenario. For shear wave excitation, the stress intensity initially increases as the distance between linings grows, and then decreases, ultimately converging to the intensity level characteristic of a single lining.

References:

[1] Lysmer J., Kyhlemeyer L., Finite Dynamik Model for Infinite Media, *Journal Engineering Mechanics Division*, ASCE, Vol.95, No.4, 1969, pp. 859-887, https://doi.org/10.1061/JMCEA3.0001144.

[2] Mirsaidov M., An account of the foundation in as-sessment of earth structure dynamics, *E3S Web of Conferences,* Vol.97, 2019, 04015, pp. 1-11, https://doi.org/10.1051/e3sconf/20199704015.

[3] Il'ichev V.A., Yuldashev, S.S., Saidov S.M., Propagation of vibration from trains in relation to track position, *Soil Mech Found Eng*, Vol.36, 1999, pp. 55–56, https://doi.org/10.1007/BF02469085.

[4] Yuldashev S.S., Karabaeva M.U., Soil surface vibrations in the training of metro trains in parallel tunnels, *Theoretical & Applied Science*, Vol. 85, No.5, 2020, pp. 117-121, https://doi.org/10.15863/TAS.2020.05.85.24.

[5] Li S., Bruna M., Djeran-Maigrea I., Kuznetsov S., Benchmark for three-dimensional explicit asyn-chronous absorbing layers for ground wave propagation and wave barriers, *Computers and Geotechnics*, Vol. 131, 2021, pp. 1-16, https://doi.org/10.1016/j.compgeo.2020.103808.

[6] Bruno Guidio, Boris Jeremic, Leandro Guidio, Chanseok Jeong, Passive seismic inversion of SH wave input motions in a truncated domain, *Soil Dynamics and Earthquake Engineering*, Vol. 158, 2022, 107263, pp. 1-47, https://doi.org/10.1016/j.soildyn.2022.107263

[7] Xavier Antoine, Anton Arnold, Christophe Besse, Matthias Ehrhardt, Achim Schadle, A Review of Transparent and Arti?cial Boundary Conditions Techniques for Linear and Nonlinear Schrodinger Equations, *Communications in Computational Physics*, Vol.4, No.4, 2008, pp. 729-796, [Online]. http://www.global-sci.com (Accessed Date: January 10, 2025).

[8] Yacine Bakhtaoui, New procedure for soil-structure interaction problems incorporating free-field effects by 2D quadratic elements, Computers and Geotechnics. Vol.165, 2024, 105843, https://doi.org/10.1016/j.compgeo.2023.105843.

[9] Pilar Velasco M., David Usero, Salvador Jim´enez, Luis V´azques, Transparent boundary conditions for the wave equation in one dimension and for a Dirac-like equation, *Electronic Journal of Differential Equations, Conference*, Vol.22, 2015, pp. 117-137, [Online]. https://ejde.math.txstate.edu/conf-proc/22/v2/velasco.pdf (Accessed Date: January 10, 2025).

[10] Miralimov M., Normuradov Sh., Ground be-haviour and settlements analysis on tunnelling of shallow-buried metro in Tashkent city, *E3S Web of Conferences*, Vol.401, 2023, 01062, pp. 1-9, https://doi.org/10.1051/e3sconf/202340101062.

[11] Adilov F., Yuldoshev B., Abirov R., Miralimov M., Numerical approach for estimation of stress-strain state of deep tunnels, *E3S Web of Conferences*, Vol.97, 2019, 04064, pp. 1-5, https://doi.org/10.1051/e3sconf/20199704064.

[12] Abirov R., Miralimov M., Calculation of the Lining of Construction of the Shallow Subway Tunnel, Hydraulic and Civil Engineering Technology VIII, M. Yang et al. (Eds.), Vol.43, 2023, pp. 42-48, https://doi.org/10.3233/ATDE230700.

[13] Ozturk K.F., Investigation of dynamic responses of three-sided underpass culvert

under near-fault and far-fault ground motions considering soil-structure interaction, *Soil Dynamics and Earthquake Engineering*, Vol.177, 2024, 108446, https://doi.org/10.1016/j.soildyn.2023.108446

[14] Bapir B., Abrahamczyk L., Wichtmann T., Prada-Sarmiento F., Soil-structure interaction: A state-of-the-art review of modeling techniques and studies on seismic response of building structures, *Front. Built Environ., Sec. Earthquake Engineering*, Vol. 9, 2023, 1120351, https://doi.org/10.3389/fbuil.2023.1120351.

[15] Silvia Falletta, Giovanni Monegato, Exact nonref-lecting boundary conditions for exterior wave equation problems, *Publications de l'institut mathématique nouvelle série*, Vol. 96, 2014, pp.103-123, https://doi.org/10.2298/PIM1410103F.

[16] Mirzaev I., Gaynazarov S., Rakhimdjanova N., Numerical solution of the wave problem in an elastic medium with transparent boundaries, *AIP Conference Proceedings*, Vol.3119, 2024, 040004, pp. 1-8, https://doi.org/10.1063/5.0214823.

[17] Kuznetsov S.V., Terentyeva E.O., Planar internal Lamb problem: Waves in the epicentral zone of a vertical power source, *Acoustic Journal*, Vol.61, No.3, 2015, pp. 387-399, https://doi.org/10.1134/S1063771015030112.

[18] Grishin A., Geraschenko V., Calculation of Ray-leigh Damping Coefficients for a Transient Struc-tural Analysis, *WSEAS Transactions on Applied and Theoretical Mechanics*, Vol. 19, 2024, pp. 49-54, https://doi.org/10.37394/232011.2024.19.5.

[19] Pedro Folhento, Rui Carneiro De Barros, Manuel Braz-César, Effect of Earthquake-Induced Structural Pounding on the Floor Accelerations and Floor Response Spectra of Adjacent Building Structures, *WSEAS Transactions on Applied and Theoretical Mechanics*, Vol.19, 2024, pp. 36-48, https://doi.org/10.37394/232011.2024.19.4.

[20] Ayoub El Amrani, Hafid Mataich, Bouchta El Amrani, Stability of Beam Bridges Under Bridge-Vehicle Interaction, *WSEAS Transactions on Ap-plied and Theoretical Mechanics*, Vol.19, 2024, pp. 55-66, https://doi.org/10.37394/232011.2024.19.6.

[21] Zienkiewicz O.C. and Morgan K., *Finite elements and approximation*, Wiley-Interscience, New York, 1983.

[22] Bathe K.J. *Finite Element Procedure Second Edi-tion*, Printed in the United States of America, 2016.

[23] Hecht F., Pironneau O., Le Hyaric A., Ohtsuka K., FreeFem++, Third Edition, Version 3 / Laboratoire Jacques-Louis Lions, Universite Pierre et Marie Curie, Paris, Freefem. A high level multiphysics finite element software, [Online]. https://freefem.org/ (Accessed Date: January 10, 2025).

Contribution of Individual Authors to the Creation of a Scientific Article (Ghostwriting Policy)

The authors equally contributed in the present research, at all stages from the formulation of the problem to the final findings and solution.

Sources of Funding for Research Presented in a Scientific Article or Scientific Article Itself

No funding was received for conducting this article.

Conflict of Interest

The authors have no conflicts of interest to declare that are relevant to the content of this article.

APPENDIX

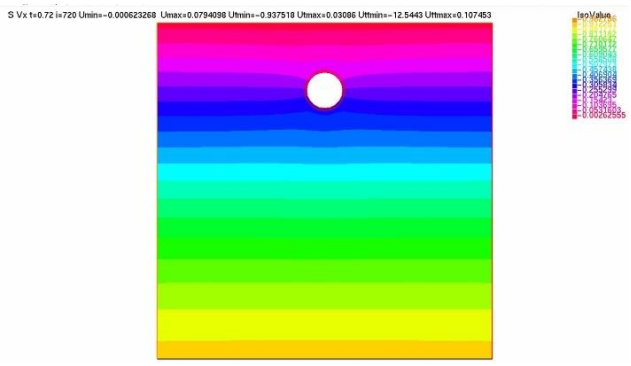

t=0.72 s

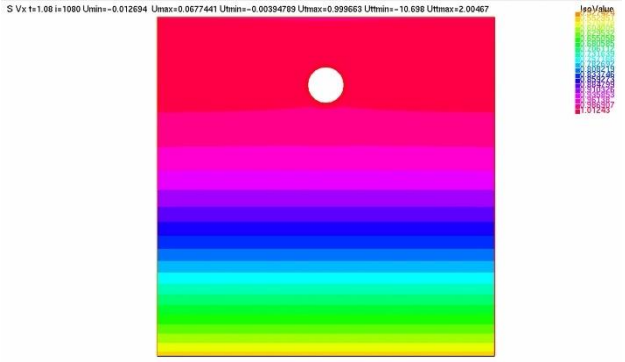

t=1.08 s

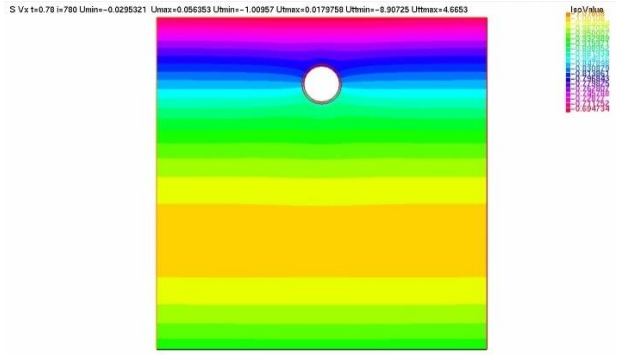

t=0.78 s

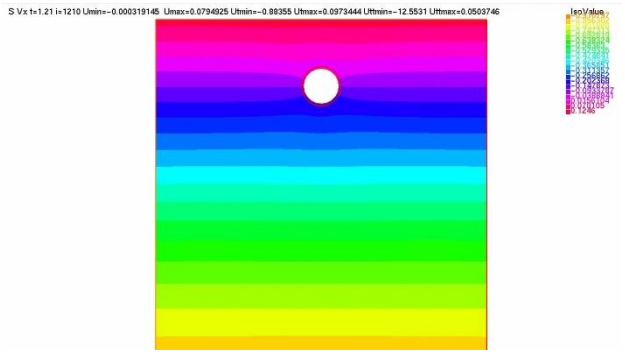

t=1.21 s

a)

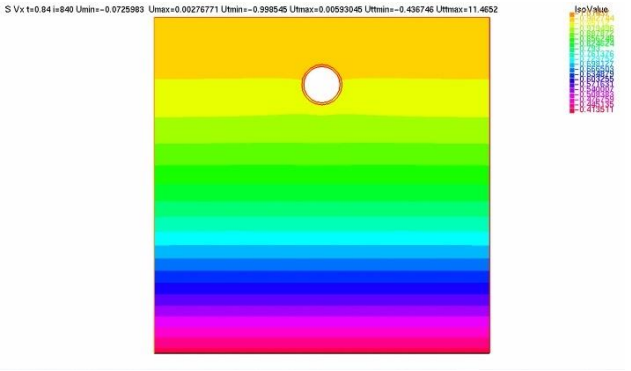

t=0.84 s

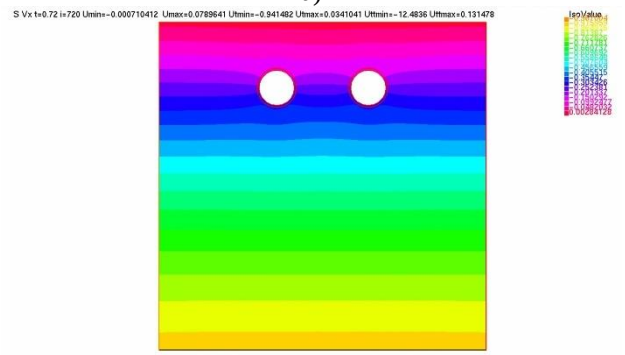

t=0.72 c

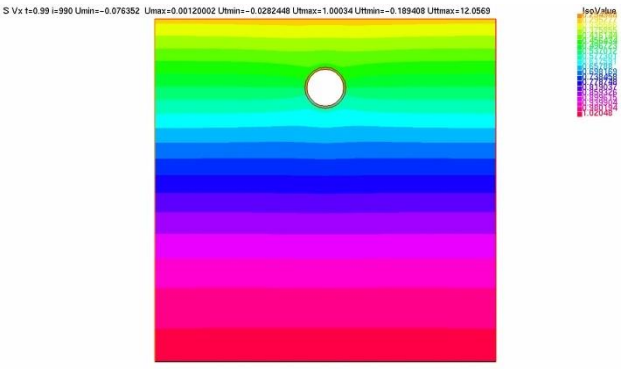

t=0.99 s

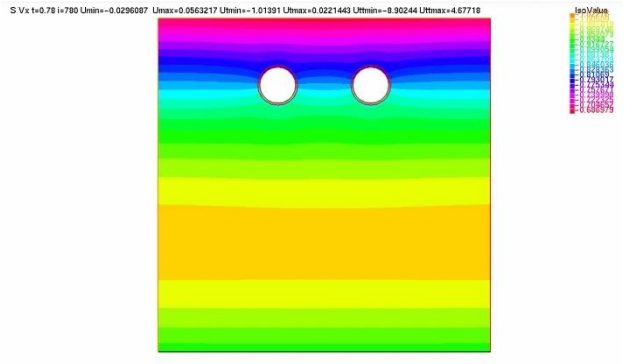

t=0.78 s

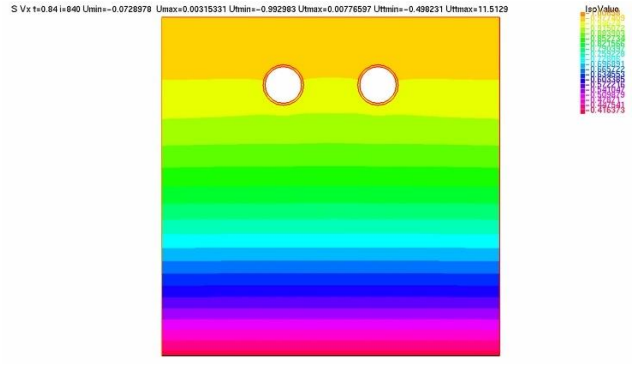

t=0.84 s

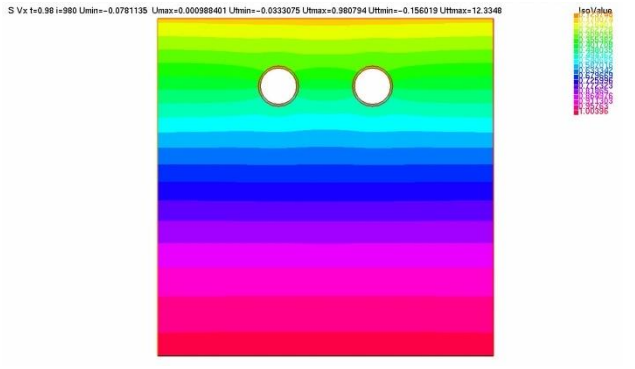

t=0.99 s

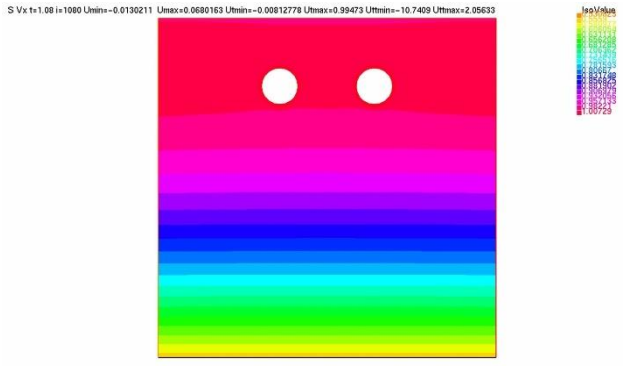

t=1.08 s

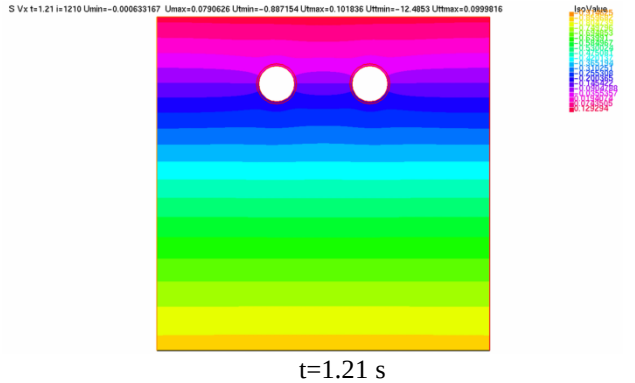

t=1.21 s

b)

Fig. 6: Dynamics of shear wave propagation in a soil medium with transparency conditions applied at artificial boundaries: a) Single lining; b) Two linings